Lymph Node Detection in IASLC-defined zones on PET/CT Images

Yihua Song[a, b], Jayaram K. Udupa*[b], Dewey Odhner[b] , Yubing Tong[b], Drew A. Torigian[b]
[a]Key Laboratory of Medical Image Computing Ministry of Education, Northeastern University, Shenyang, Liaoning, China; [b]Medical Image Processing Group, Department of Radiology, University of Pennsylvania, Philadelphia, PA19104, USA.

ABSTRACT

Lymph node detection is challenging due to the low contrast between lymph nodes as well as surrounding soft tissues and the variation in nodal size and shape. In this paper, we propose several novel ideas which are combined into a system to operate on positron emission tomography/ computed tomography (PET/CT) images to detect abnormal thoracic nodes. First, our previous Automatic Anatomy Recognition (AAR) approach is modified where lymph node zones predominantly following International Association for the Study of Lung Cancer (IASLC) specifications are modeled as objects arranged in a hierarchy along with key anatomic anchor objects. This fuzzy anatomy model built from diagnostic CT images is then deployed on PET/CT images for automatically recognizing the zones. A novel globular filter (g-filter) to detect blob-like objects over a specified range of sizes is designed to detect the most likely locations and sizes of diseased nodes. Abnormal nodes within each automatically localized zone are subsequently detected via combined use of different items of information at various scales: lymph node zone model poses found at recognition indicating the geographic layout at the global level of node clusters, g-filter response which hones in on and carefully selects node-like globular objects at the node level, and CT and PET gray value but within only the most plausible nodal regions for node presence at the voxel level. The models are built from 25 diagnostic CT scans and refined for an object hierarchy based on a separate set of 20 diagnostic CT scans. Node detection is tested on an additional set of 20 PET/CT scans. Our preliminary results indicate node detection sensitivity and specificity at around 90% and 85%, respectively.

Keywords: IASLC classification, lymph nodes, lung cancer, Automatic Anatomy Recognition (AAR), fuzzy models.

1. INTRODUCTION

The accurate assessment of lymph node involvement is important for the management of lung cancer for cancer staging and effective treatment monitoring [1]. Features such as the number of enlarged nodes, the size or volume of nodes, and the presence and degree of nodal radiotracer uptake in PET images are important as disease biomarkers. Previous studies proposed several methods for the automated detection of lymph nodes. For example, Kitasaka et al [2] proposed a 3D minimum directional difference filter to detect abdominal lymph nodes in CT images automatically. Feulner et al proposed a method combining a discriminative model with prior anatomical knowledge that is modeled as a spatial probability [3]. Liu et al [4] proposed a ball-scale Hessian analysis method to use shape features to detect lymph nodes on chest and abdominal images. Barbu et al [4] adopted a method combining with a machine learning method to detect and segment lymph nodes on CT images. The detection of lymph nodes in the thorax is challenging because nodal CT appearance is similar to that of soft tissue, and nodal shape and size have similarity to the vessels and esophagus. The International Association for the Study of Lung Cancer (IASLC) has defined [6] a standard way of zoning lymph node clusters to help in standardizing disease measurement and reporting. This standard is beginning to be implemented in computerized methods for detecting and quantifying the disease burden [7].

In this paper, we extend our previous method [7] of localizing IASLC-defined zones on CT images to PET/CT images. If disease can be measured accurately on PET/CT images, it would become possible to characterize disease in terms of metabolic activity (PET) and anatomic appearance (CT). We present a new strategy in this paper which combines information gathered at different scales for detecting and quantifying diseased lymph nodes. The approach employs a new filter called globular filter (g-filter) to identify explicitly globular blobs of differing sizes on PET/CT images.

Unlike published methods, our strategy takes a global-to-local approach where zones are first recognized (localized) using our Automatic Anatomy Recognition (AAR) approach and then the nodes are detected within the zones as

Medical Imaging 2016: Computer-Aided Diagnosis, edited by Georgia D. Tourassi, Samuel G. Armato III,
Proc. of SPIE Vol. 9785, 978515 · © 2016 SPIE · CCC code: 1605-7422/16/$18 · doi: 10.1117/12.2217767

described in Section 2. We report the experimental results of our proposed method in Section 3, followed by some discussions and conclusions in Section 4.

2. METHODS

We modify the previously developed AAR framework [8] for lymph node detection. In this modification, we treat lymph node zones as anatomic objects (even though they are not presented with boundaries in any image), model the zones keeping key anatomic organs as anchor objects of reference, automatically localize the organs and zones, and finally detect lymph nodes within each recognized zone by making combined use of the zonal location, CT and PET image information, and the response from a bank of globular filters.

This retrospective study was conducted following approval from the Institutional Review Board at the Hospital of the University of Pennsylvania along with a Health Insurance Portability and Accountability Act waiver. Contrast-enhanced diagnostic chest CT scans of 45 near normal subjects (radiologically normal with exception of minimal incidental focal abnormalities), 10 ^{18}F-fluorodeoxyglucose (FDG)-PET/CT scans of near normal subjects with no lymph node disease involvement, and 10 FDG-PET/CT scans of patients with different diseases with involvement of thoracic lymph nodes are utilized in our study.

The methodology consists of five main steps. First, we build fuzzy models of the anatomic objects and zones from the above mentioned diagnostic CT images following the hierarchy AAR methodology [8]. Second, the best hierarchical arrangement to be used for objects (organs and zones) so as to yield optimal zonal recognition accuracy is determined. Third, the globular filter is applied to each recognized zone to detect blob-like structures within the zone. Finally, combining the prior information and the results we obtained from the previous step, abnormal lymph nodes are detected. These steps are described below.

2.1 Model building

The thoracic organs as defined in [8] and IASLC mediastinal zones as defined in [6] along with addition of axillary zones are considered in this study. They are as follows. Organs: Outer skin boundary of the thoracic body region (TSkn), left and right pleural spaces (LPS & RPS), thoracic skeleton (TSk), pericardium (PC), trachea & bronchi (TB), respiratory system (RS = LPS + RPS + TB), esophagus (E), arterial system (AS), venous system (VS), spinal cord (SCrd). Lymph node zones: AxillaL and AxillaR (left and right axillary nodes each as a zone), and IASLC-defined zones: Zone1, Zone2L, Zone2R, Zone3a, Zone3p, Zone4L, Zone4R, Zone5, Zone6, Zone7, Zone8, and Zone9.

Each of the above 24 objects (organs and zones) was delineated using interactive tools under expert supervision and verification strictly following the definition of the objects given in [8] and [6]. From these delineations, a fuzzy anatomy model $FAM(B)$ of the thoracic body region B was built as $FAM(B) = (H, M, \rho, \lambda, \eta)$ as per the methodology in [8] by treating zones as well as the organs as objects. The elements of $FAM(B)$have the following meaning. H is a hierarchy, represented as a tree, of the objects (organs and zones) considered in B for inclusion in the anatomy model. M is a collection of fuzzy models, one fuzzy model for each object in B. ρ describes the relationship of parent to offspring in H. λ is a set of scale factor ranges indicating the size variation of each object in B. η represents a set of measurements pertaining to the objects in B.

2.2 Zone recognition

Our goal is to accurately recognize (localize) zones and then detect nodes within each zone for disease quantification. For our initial investigation (because of the small number of test images and hence the small number of nodes falling in each zone), we grouped zones (rather than treat each zone separately) as follows: Axilla = AxillaL + AxillaR, Zone234 = Zone2 + Zone3 + Zone4, Zone56 = Zone5 + Zone6, Zone789 = Zone7 + Zone8 + Zone9.

The hierarchy H chosen can have significant influence on the accuracy of object localization/recognition. The variabilities observed in ρ and λ are used to make informed decisions about the choice of appropriate parent organs for different zones. To this end, we have used skin object (TSkn) as the root object, and each of the other organs as the root's offspring to test which offspring organ yields the best recognition result for each grouped zone in a simple hierarchy illustrated in Figure 1. Of the 45 normal diagnostic CT image data sets, 25 were used for model building and the remaining 20 were used for testing nodal zone recognition for determining the best hierarchy in this manner.

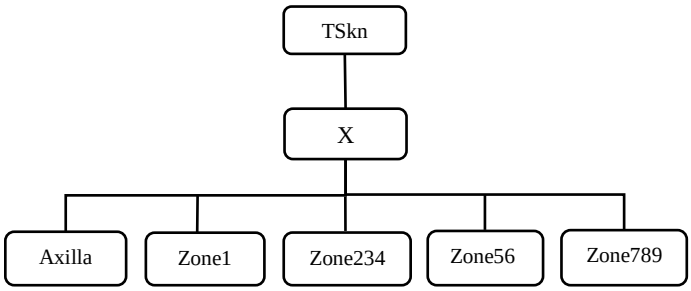

Figure 1. Testing the suitability of different organs (denoted by X) as parent for each grouped zone.

Two recognition approaches are applied for recognition, the one-shot method [9] and the thresholded optimal search method [8]. In this work, these two strategies are implemented in combination to recognize different objects. Because we can refine object pose via intensity-based information, we use the thresholded optimal search algorithm to recognize objects TSkn, TSk, and TB, since these objects manifest themselves with appearance and boundary information. Since zones do not present in the images with specific appearance or boundary information they are recognized by using the one-shot method.

To choose the best hierarchy, we used the metrics of distance error. Distance error is the distance between the geometric centers of the known true delineated object and the fuzzy model when the object is recognized. Following the arrangement in Figure 1, the organ X which yields the smallest distance error for each zone is taken to be the parent or anchor organ for that zone. The best overall hierarchy H for $FAM(B)$ is then determined to be the hierarchy with TSkn as the root and with each subtree rooted at TSkn to consist of the best parent organ found for a zone followed by the zone.

Once the best hierarchy is determined in this manner, the model along with the hierarchy built from diagnostic CT data sets was deployed on the 20 PET/CT data sets images for testing nodal detection. The best hierarchy arrived at is shown in Figure 2. Grouped zones are recognized on the low-dose CT (*l*CT) images of PET/CT acquisitions. Then, the nodes are detected within each recognized grouped zone as described below.

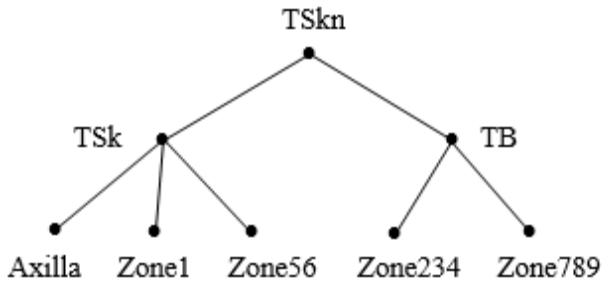

Figure 2. The best hierarchy found by the method described in text.

2.3 Lymph node detection

Lymph nodes in the thoracic region are very difficult to detect only based on appearance because all lymph nodes have attenuation coefficients similar to muscles and vessels. However, both muscles and vessels generally have a longer spatial extent and larger volume within the body. Furthermore, we know that the size of lymph nodes can vary considerably, and that pathological lymph nodes are typically enlarged, often appearing in merged clusters. Keeping these aspects of prior knowledge in mind, we combine the following characteristics of lymph nodes within the proposed approach to detect candidate lymph nodes.

1) Lymph nodes are not inside any organ in the body, so that the space inside any organ can be excluded from the search region.

2) Although lymph nodes are surrounded by fat tissue, the intensity distribution is not uniform for either the nodes or the background.

3) The attenuation of lymph nodes in CT images is close to that of muscles and vessels. Therefore, if they can be distinguished from muscles and vessels by shape, a threshold interval can be used to define them. Also, the intensity of abnormal lymph nodes in PET images is much higher than that of other surrounding regions.

Hence, the above prior knowledge is embedded into our system to help to greatly reduce the number of false detections and thus improve true positive detections.

Following the previous step of zone recognition, for each (grouped) zone z, we have four items of information available within z's fuzzy mask for each voxel v: its CT gray scale value $f_{CT}(v)$, its PET (standardized uptake value (SUV)) value $f_{PET}(v)$, its zonal membership value from the fuzzy model $f_M(v)$, and its g-filter output $f_g(v)$. The latter quantity consists of two values $f_g(v) = (\delta(v), r(v))$, where δ is the optimal g-filter response and r is the optimal g-filter size. These are estimated as follows.

At each voxel v, each ball b from a series of balls centered at v of radius from a pre-determined minimum r_{min} to maximum r_{max} is considered and the ball that yields the best separation between the histogram of intensities inside b and just outside b is found. The radius of this ball is taken to be r and the best separation is considered to be δ. The values for r_{min} and r_{max} are chosen so as to cover all nodal sizes that are encountered in practice. The g-filter is applied to the *l*CT image in this work (although it can also be applied to the PET image). At true nodal "centers", we expect δ to peak, so we find local maxima as potential nodal locations. True nodal locations are then selected from these locations by employing a simple thresholding strategy in this initial study: v is a local maximum and its optimal ball satisfies a threshold criterion for $f_{CT}(v)$, $f_{PET}(v)$, and $f_M(v)$. The node size at v is considered to be r. Many more refined strategies are possible for node detection and subsequent delineation toward the goal of disease quantification.

3. EXPERIMENTAL RESULTS

The proposed method has been evaluated on 20 PET/CT datasets of the chest. For testing the best hierarchy, contrast-enhanced CT image data sets of 45 near normal subjects are utilized. Image data sets from 25 of these subjects are used for model building and the remaining are used for testing the AAR recognition performance of all the zones. In these data sets, voxel size = $0.9 \times 0.9 \times 5$ mm^3, and image size = $512 \times 512 \times 51 - 69$. For the 20 PET/CT data sets, all *l*CT datasets were resampled to an isotropic 1.17 x 1.17 x 4 mm^3 resolution to match with PET images. The image size of *l*CT and PET = $(428 - 512) \times (428 - 512) \times 51 - 69$ mm^3.

Sample recognition results for the grouped zones are displayed in Figure 3 by overlaying the cross sections of the fuzzy model at recognition on a slice of the *l*CT and matching PET images containing pathology. The recognition results have been visually found to be satisfactory in all 20 PET/CT studies as per IASLC definitions.

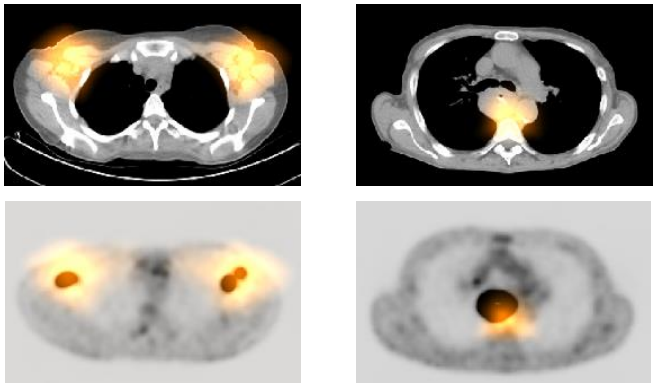

Figure 3. Sample zone recognition results for Thorax. Axilla (left column) and Zone789 (right column) overlaid on *l*CT (top row) and PET images (bottom row) containing pathologic lymph nodes.

Some sample node detection results are displayed in Figure 4 where cross sections of the optimal balls are overlaid on *l*CT slices and the detected nodes are indicated by arrows. Note the variation in size and shape of the nodes. Although the shapes are not perfectly spherical, the g-filter together with the entire AAR strategy for first localizing zones and then making combined use of PET and CT information was able to detect the nodes. Figure 4 shows examples of true positive

and false positive lymph node candidates. The proposed approach achieved node detection sensitivity and specificity at around 90% and 85% respectively. Table 1 lists our preliminary results for node detection on the 20 PET/CT images from two grouped zones – Axilla and Zone789.

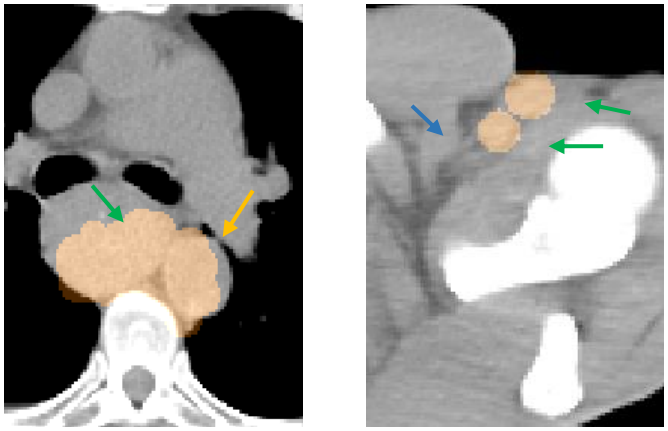

Figure 4. Sample lymph node detections results for Zone789 (left) and Axilla (right). Arrows point to false negative (blue), false positive (yellow), and true positive (green) detections.

Table 1. Lymph node detection results for Axilla and Zone789

Zone	Number of nodes	False positive	False negative
Axilla	10	1	2
Zone789	10	3	0

4. CONCLUSION

Lymph node detection especially in PET/CT images, is challenging due to the low contrast between lymph nodes and surrounding soft tissues and the variation in their size and shape. In this paper, we proposed several novel ideas which are combined into a system. The ideas include: automatic localization of the nodal zones following our AAR approach where zones are treated as objects, g-filter to locate and detect the presence of blob-like objects, and combined use of *l*CT, PET, object model, and g-filter response to detect and delineate diseased nodes.

In this work, proper lymph node zonal recognition is crucial for effective lymph node detection. However, lymph node zones do not need to be precisely delineated, which is a rather ill-defined and challenging problem. The effectiveness of zone recognition is influenced by the anchor objects and the hierarchy chosen in fuzzy model building. Effective lymph node detection is facilitated by the combined use of different items of information at various scales: model at recognition indicating geographic layout at the global level of nodal clusters, g-filter output which hones in on and carefully selects node-like globular objects at the node level, and CT and PET gray value but within only the most plausible regions for node presence at the voxel level. This combined strategy sets this approach apart from previous approaches to lymph node detection.

REFERENCES

[1] American Cancer Society, Cancer Facts& Figures 2016. Atlanta: American Cancer Society; 2016. http://www.cancer.org/research/canerfactsstatistics/canerfactsfigures2016/index (2016).

[2] Takayuki K, Yukihiro T, Nakamura Y, Mori K, Suenaga Y, Ito M, Nawano S, Automated extraction of lymph nodes from 3-D abdominal CT images using 3-D minimum directional difference filter. MICCAI 2007;4792: 336- 343.

[3] Feulner J, Zhou SK., Hammon M., Hornegger J, Comaniciu D. Lymph node detection and segmentation in chest CT data using discriminative learning and a spatial prior. Med Image Anal. 2013 Feb;17(2):254-70.

[4] Liu J, Hua J, Yao J, White JM, Summers RM. Computer-aided Abdominal Lymph Node Detection Using Contrast enhanced CT Images. Proc SPIE 2011; 7963:796313-1 -796313-7.
[5] Barbu A, Suehling M, Xu X, Liu D, Automatic Detection and Segmentation of Axillary Lymph Nodes. MICCAI 2010;6361:28-36.
[6] Rusch VW, Asamura H., Watanabe H, et al. The IASLC lung cancer staging project: a proposal for a new international lymph node map in the forthcoming seventh edition of the TNM classification for lung cancer. J Thorac Oncol 2009;4(5): 568-577.
[7] Matsumoto MMS, Beiga N, Udupa JK, Archer S, Torigian DA, Automatic localization of IASLC-defined mediastinal lymph node stations on CT images using fuzzy models, Proc SPIE 2014:9035:90350J-1-90350J-7.
[8] Udupa JK, Odhner D, Zhao L, et al. Body-wide hierarchical fuzzy modeling, recognition, and delineation of anatomy in medical images. Med Image Anal 2014;18(5)752-71.
[9] Udupa JK, Odhner D, Tong Y, Matsumoto MMS, Ciesielski KC, Vaideeswaran P, Ciesielski V, Saboury B, Zhao L, Mohammadianrasanani S, Torigian DA. Fuzzy model-based body-wide anatomy recognition in medical images. Proc SPIE 2013:8671:86712B-1-86712B-7.